GENERAL PHYSICS

I. MOLECULAR BEAMS*

Academic and Research Staff

Prof. J. R. Zacharias	Dr. G. A. Herzlinger	Dr. J. C. Weaver
Prof. J. G. King	Dr. E. H. Jacobsen	J. H. Abrams
Dr. J. W. Coleman	Dr. M. G. R. Thomson	F. J. O'Brien

Graduate Students

J. E. Bergmann	H. F. Dylla	D. G. Lysy
M. D. Brody	J. A. Jarrell	N. D. Punsky
S. A. Cohen	S. R. Jost	B. R. Silver

RESEARCH OBJECTIVES

1. Molecule Microscopy

We are continuing our work in microscopy, the object of which is (i) to study surface variations of weak forces (sites) by desorbing previously adsorbed neutral molecules by means of a technique that we call neutral molecule surface staining; (ii) to develop a new form of microprobe that is likely to be competitive with the ion and x-ray devices already in existence; and (iii) to study emissions of vapor and gas from biological samples. These emissions may occur spontaneously or as a result of electrical, chemical, or radiation stimuli.

There are many forms that this instrumentation can take, depending on the problem to be studied. Different provisions can be made for dead or live samples. The instrument can be built to have spatial resolution of varying degrees, temporal resolution, or mass resolution (i.e., the identification of emerging molecules by ionizing them and identifying them mass spectrometrically). The neutral emissions from the sample may occur simply as a result of the temperature of the sample, or after heating small areas with beams of charged particles or light, in which case the resolution can be that associated with the stimulating beam.

We are continuing our collaboration with various scientists in the Boston area. Our collaborators include Dr. S. Caplan (Harvard Medical School), Dr. A. Essig (New England Medical Center), and Professors P. Robbins and D. Waugh (Department of Biology, M.I.T.).

2. Electron Microscopy

Work is continuing on high-resolution high-contrast electron microscopy. This project involves the development of new kinds of electron lenses using foils. Facilities for testing foils and various lens configurations are being set up.

J. G. King

*This work is supported by the Joint Services Electronics Programs (U.S. Army, U.S. Navy, and U.S. Air Force) under Contract DAAB07-71-C-0300, the National Institutes of Health (Grant 5 SO5 FR07046-06), and by Public Health Service Research Grant 1 PO1 HL14322-01 from the National Heart and Lung Institute to the Harvard-M.I.T. Program in Health Services and Technology.

(I. MOLECULAR BEAMS)

A. STIMULATED DESORPTION BY LOW-ENERGY ELECTRONS

Joint Services Electronics Programs (Contract DAAB07-71-C-0300)

H. F. Dylla, G. A. Herzlinger

One of the main efforts of the Molecular Beams laboratory is the development of a device (the scanning desorption molecule microscope) for studying the spatial distribution of various molecular species adsorbed to surfaces.

As part of this work, we are investigating the use of stimulated desorption by low-energy electrons (0-500 eV). These electron-stimulated desorption (ESD) studies are also applicable to problems of catalysis, upper atmospheric and interstellar physics, plasma containment, and microelectronic circuitry.

Although there has been much interest in electron-stimulated desorption, most previous investigators have dealt with the desorption of chemisorbed gases (CO, O_2) from metal surfaces.[1] We plan to study nonmetallic as well as metallic substrates, and employ both physisorbed and chemisorbed adsorbates. We also plan to extend ESD techniques to the study of the surface chemistry of a variety of insulators. We have begun to investigate the desorption of neutrals, positive ions, and negative ions from various substrate-adsorbate systems. Desorbed negative ions have been ignored in most ESD investigations, even though many interesting negative-ion reactions have been observed in gas-phase studies in the 1-10 eV energy regime. In this report we describe our initial efforts to make direct measurements of the desorption of neutrals, which is a difficult task because the detector efficiency and solid-angle subtention are usually comparatively small quantities with unknown values.

Slow electrons interact primarily with the adsorbed atoms without affecting the substrate, unlike the situation when ionic sputtering and similar techniques are used. The desorption effects are observed at such small incident power densities (typically 10^{-3}-10^{-5} W/cm^2) that thermal effects are not important. Both desorbed positive ions and neutrals have been detected, and the chemisorption studies indicate that the cross sections for such processes are energy-dependent and specific to the particular species involved. The ionic cross sections are of the order of 10^{-19}-10^{-23} cm^2, and thus are several orders of magnitude lower than the free molecular ionization cross sections. Total desorption cross sections, which include all processes that deplete the surface coverage, including desorption of ions, neutrals, excited neutrals, and conversion to different binding states, are found to be 50 to 10^5 times larger than the corresponding ionic cross sections. Most reported measurements of the total desorption cross section Q are deduced from the measured decrease of the desorbed ion current as a function of time

$$i^+ = i_o^+ \exp\left[-\frac{i_e Q t}{A e}\right]. \qquad (1)$$

The difference between the value of Q calculated in this manner and the measured value of the ionic cross section Q^+ is the value usually quoted for the neutral cross section. Implicit in such a measurement are the assumptions that the total cross section and ionic cross section are coverage-independent, and that the electron-induced conversion of binding states can be ignored. Direct measurements of the desorption of neutrals would be valuable.

The mechanisms involved in electron-stimulated desorption are not well understood,[2,3] but it is thought that some of the processes involved are excitation to antibonding states in analogy with a diatomic molecule, direct surface ionization followed by desorption, and excitation to a metastable state followed by relaxation to an ionized state. Studies of threshold electron energy[3] indicate that ions and neutrals are produced by the same process, and that Auger neutralization of the surface ions is an important effect.

The reduced cross sections observed for ionic desorption from metallic substrates is probably the result of rapid Auger neutralization of the surface ions. Hagstrum[4] has demonstrated the efficiency of such neutralization processes by bombarding metallic and semiconductor surfaces with low-energy ions. The tunneling of electrons from the valence bands of semiconductor substrates was found to be nearly as probable as tunneling of conduction electrons from metals. Such processes are much less likely to occur with insulating substrates because of the large energy gap between the conduction and valence bands. In the past, electron-stimulated desorption studies with insulators have been limited to several ionic crystals.[5] In extending ESD techniques for insulators, we anticipate these practical problems: surface charging, electron radiation damage, and maintenance of surface cleanliness. Excessive charging and electron radiation damage of the substrate will probably not be serious because of the low power densities that are required to desorb measurable quantities of adsorbate. If the charging problem should prove serious it could probably be eliminated by the use of a thin substrate supported by a conductor. It is difficult to predict the extent of possible electron radiation damage to the substrate because we lack quantitative damage studies with low-energy, low-power electron beams. To insure cleanliness of the substrate surface before exposure to a particular adsorbate, we anticipate that the substrate will have to be prepared in vacuo or in a solvent that is subsequently desorbed or evaporated in vacuo.

In our initial experiments with the desorption of adsorbed H_2O from a polished copper surface, we have observed some of the phenomena described by other researchers, especially the strong H^+ signal.

Our preliminary studies are being carried out with the apparatus shown in Fig. I-1.

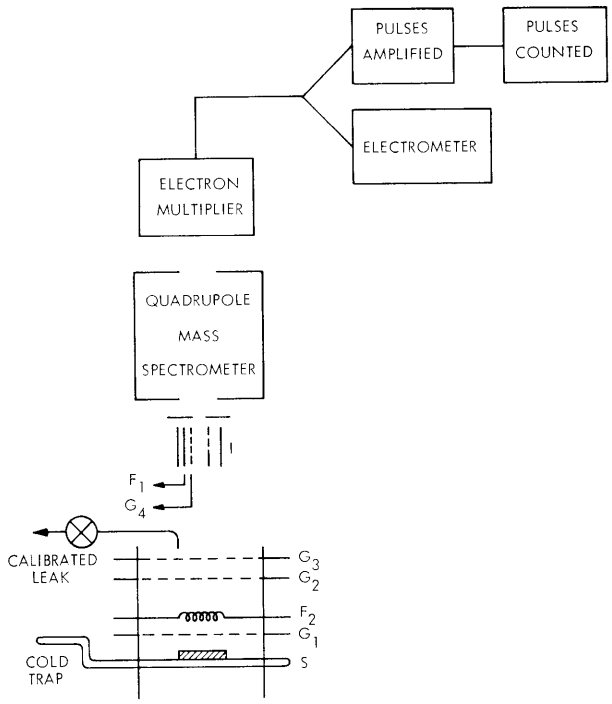

Fig. I-1. Apparatus for electron-stimulated desorption studies.

The substrate (S) is irradiated by low-energy electrons from a thoriated tungsten filament (F_2), of 5 mil diameter. The filament can be floated at some negative potential (0-500 V) relative to the potential of the substrate. Neutrals desorbed from the substrate are ionized in a high-efficiency ionizer (I) of the type described by Brink.[6] The resulting ions are mass-analyzed by a quadrupole mass spectrometer and detected with a 14-stage Cu-Be electron multiplier. The output pulses from the multiplier are either amplified and counted, or directly integrated with an electrometer if the pulse rate exceeds 10^5 c/s. Grid G_1 is used for modulating the intensity of the desorbing electrons. Grids G_2 and G_3 are used for discriminating against ions produced in the gas phase above the substrate, and for focusing desorbed ions when ionic measurements are made. The substrate is clamped to a cold trap for cooling to 77°K, and can be exposed to various adsorbate gases by a calibrated leak. The apparatus is contained in a Pyrex stainless-steel vacuum system pumped by a zeolite-baffled diffusion pump and liquid nitrogen cold traps. System pressures of 2×10^{-8} Torr can be obtained with only moderate baking of the Pyrex walls (100°C for 24 hours). Lower pressures will probably require proper baking of the stainless-steel flanges and viton "O" rings that seal the system. A sample holder-vacuum lock arrangement for rapid change of samples has been added to the system and will be used in the future.

References

1. T. E. Madey and J. T. Yates, J. Vac. Sci. Tech. 8, 525 (1971).
2. D. Menzel and R. Gomer, J. Chem. Phys. 41, 3311 (1964).
3. P. A. Redhead, Can. J. Phys. 42, 886 (1964).
4. H. D. Hagstrum, Phys. Rev. 119, 940 (1960); D. D. Pretzer and H. D. Hagstrum, Surface Sci. 4, 265 (1966).
5. P. W. Palmberg and T. N. Rhodin, J. Phys. Chem. Solids 29, 1917 (1968).
6. G. O. Brink, Rev. Sci. Instr. 37, 857 (1966).

B. SUPERFLUID HELIUM CRITICAL VELOCITY MODEL

Joint Services Electronics Programs (Contract DAAB07-71-C-0300)

J. C. Weaver

Development of a simple Feynman-type critical velocity model for the onset of dissipation of superfluid helium in small ($\leq 5 \times 10^{-4}$ cm), irregular channels has yielded the following expression[1] for the low temperature ($T \ll T_\lambda$) critical velocity:

$$v_o \approx \frac{k}{2\pi(D+\delta)} \left\{ \ln \left(\frac{D+\delta}{\pi a} \sin \frac{\pi D}{D+\delta} \right) + \frac{1}{4} \right\}. \tag{1}$$

Here D and δ are the channel parameters shown in Fig. I-2, k is the quantum of circulation, and a is the core radius of a quantized vortex line. For $D \approx \delta$ Eq. 1 gives values of v_o that are in much better agreement with experimental data[2-4] in the

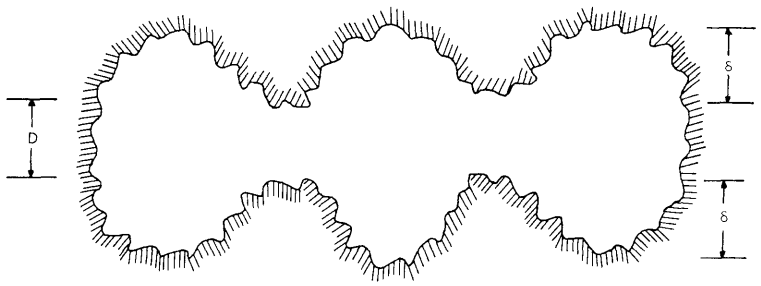

Fig. I-2. Channel cross section of an irregular channel containing superfluid flow directed into the paper. The irregular nature of the channels is modeled by specifying a channel size D and a surface roughness parameter δ. D is the typical minimum vertical spacing between the peak surface roughness variations, while δ is the peak height of the combined major and minor surface modulations that represent the channel roughness.

temperature region well below T_λ than those predicted by previous Feynman-type models.[5-8] These previous models have treated simpler and cleaner geometries, and hence the geometry does not quantitatively include surface roughness. Actual experiments, however, are conducted with materials such as filter paper, Vycor glass or packed fine powder and are usually characterized by surface roughness of the same order as the channel size. A recent model for dissipation caused by inhomogeneous nucleation of vortex rings has been proposed by Hess.[9] This model does include surface roughness modeled by adsorbed spherical dust grains, but depends on grain size only, with no explicit channel size dependence as does the present model.

Helpful conversations with M. G. R. Thomson and J. G. King are gratefully acknowledged.

References

1. J. C. Weaver (Ms in preparation).
2. J. R. Clow and J. D. Reppy, Phys. Rev. A 5, 424 (1972).
3. G. Kukich, R. P. Henkel, and J. D. Reppy, Phys. Rev. Letters 21, 197 (1968).
4. H. Kojima, W. Vieth, S. J. Putterman, E. Guyon, and I. Rudnick, Phys. Rev. Letters 27, 714 (1971).
5. R. P. Feynman, in C. J. Gorter (Ed.), Progress in Low Temperature Physics, Vol. 1 (North-Holland Publishing Company, Amsterdam, 1955), p. 17.
6. W. I. Glaberson and R. J. Donnelly, Phys. Rev. 141, 208 (1966).
7. W. F. Vinen, in G. Careri (Ed.), Liquid Helium (Academic Press, Inc., New York, 1963), p. 336.
8. J. C. Weaver, Phys. Rev. A 6, 378 (1972).
9. G. B. Hess, Phys. Rev. Letters 29, 96 (1972).

C. DETECTION OF QUANTIZED VORTEX LINES IN SUPERFLUID HELIUM AT A KNOWN PINNING SITE

Joint Services Electronics Programs (Contract DAAB07-71-C-0300)

E. Bogatin, S. R. Jost, J. C. Weaver

Quantized vortex lines are among the fundamental and unique properties of superfluid helium. By measuring the circulation around a fine wire, Vinen[1] first observed quantized flow in superfluid; similarly, Rayfield and Reif[2] were the first to demonstrate experimentally the presence of quantized vortex rings (which are lines closed upon themselves). More recently, a rather elegant but conceptually simple experiment by Packard and Sanders[3] supported the existence of vortex lines. By observing the negative charge trapped in the superfluid in a rotating capillary as a function of angular velocity Ω, they noted step increases in the collected trapped charge, with each step attributed to line

formation somewhere within the capillary.

Our experiment[4,5] adds a unique and important feature to this last work: because of free-energy considerations, the first vortex tends to form between two axial needles (pinning sites) in a capillary tube (see Fig. I-3). If k is the quantum of circulation, ℓ_T is the length of the capillary tube, and a_o is the vortex core radius (~1 Å), then the free energy, $F = E - \Omega L$, of this system in rotation with a pinned vortex line is a simple function of the needle lengths:

$$F = \rho_s k \left\{ \frac{k}{4\pi} (\ell_T \ln [R/a_o] - (\ell_e + \ell_c) \ln [a/a_o]) - \frac{\Omega}{2} \left(R^2 \ell_T + (\ell_c + \ell_e) a^2 \right) \right\} . \quad (1)$$

Here ℓ_c and ℓ_e are the lengths of the collector and emitter needles, respectively, R is the radius of the capillary tube, a is the radius of the needles, and ρ_s is the superfluid helium density. By replacing the high-velocity core region of the vortex with the needle shanks we lower the free energy of the system and thereby induce the vortex line to form

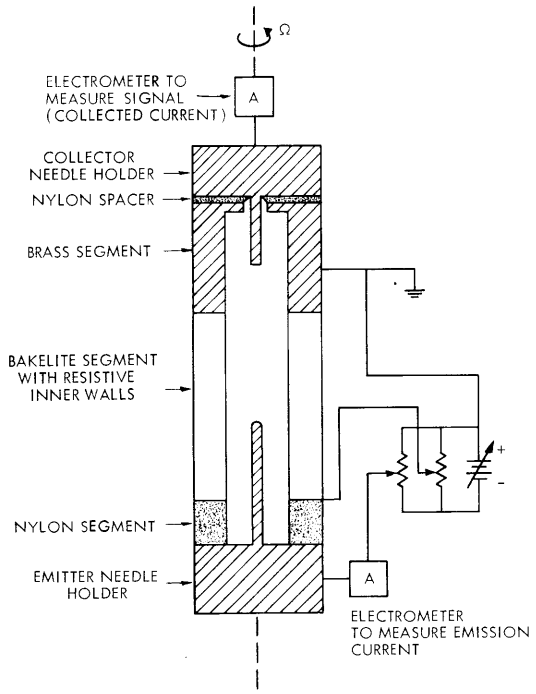

Fig. I-3.

Basic apparatus showing major details of construction. Only the capillary rotates; electrical leads are brought out to the indicated circuits via mercury troughs.

between the pinning sites. Upon formation, the vortex line traps electrons[6,7] along its length, and causes an axial space-charge buildup which tends to inhibit the emission of electrons and also provides an extra deflection of electrons away from the collector. Both effects decrease the collected current, and such decreases have been observed (Fig. I-4).

Initially, before a pinned vortex line forms, the free energy is zero, since the superfluid velocity is zero everywhere. The angular velocity at which the vortex can first

form occurs when F given by (1) becomes equal to the free energy of the initial, vortex-free state, that is, zero. Thus, the theoretical value of Ω at which vortex formation can first occur is given by

$$\Omega_{\text{theory}} = \frac{k}{2\pi}\left\{\frac{\ell_T \ln [R/a_o] - (\ell_c+\ell_e) \ln [a/a_o]}{R^2\ell_T + (\ell_c+\ell_e)a^2}\right\}. \tag{2}$$

Note that Ω_{theory} is independent of ρ_s, and therefore T, but depends directly on $(\ell_c+\ell_e)$ for a given value of ℓ_T. Also, Ω_{theory} is the lowest value of Ω at which a vortex line can form; superfluid helium flows are known to be metastable, so that actual vortex formation can, and often does, occur at Ω somewhat larger than Ω_{theory} (Figs. (I-5 and I-6).

The apparatus has 3 cylindrical segments axially bored to an inside diameter of 0.25 cm. The needle holders are located at both ends and allow for the adjustment of the needle lengths in the apparatus so that we can observe the dependence of angular velocity of formation on the needle lengths. The primary segment of the apparatus is bakelite, and has inner walls coated with a carbon film to provide a continuous accelerating field for the electrons from the emitter to the collector. The fields draw nonaxial electrons to the walls and leave a collected current that is responsive to axial phenomena. The brass segment shields the collector from pickup and the nylon segment insulates the emitter so that emission current measurements may be made. We used a stationary cryostat and mounted the apparatus on a shaft that enters the cryostat through a rotating vacuum bearing. The signal lead is a spring-loaded steel wire which was incorporated

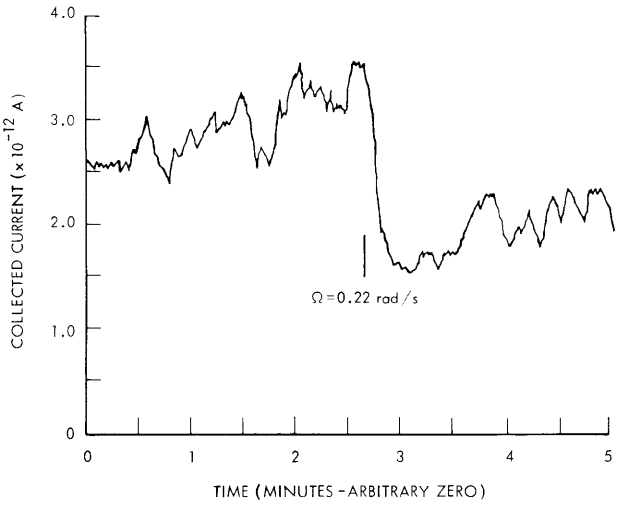

Fig. I-4. Vortex formation during slow angular acceleration of the apparatus. The decrease in collected current associated with formation of a vortex line between the needles occurred at $\Omega = 0.22$ rad/s^{-1}.

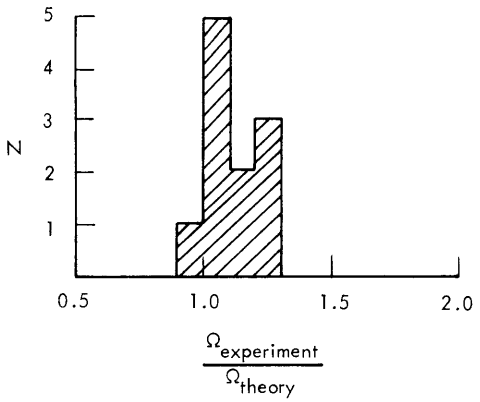

Fig. I-5. Experimental critical angular velocity normalized to the theoretical value. Since the theoretical value depends on $(\ell_c + \ell_e)$ which was varied (see Fig. I-6), this normalization was used in order to compare all points on a common basis. Each run yields one point and requires approximately 3 hours. Runs for which the maximum Ω was less than Ω_{theory} and for which no vortex formation occurred, and runs for which $T \geq 1.74°K$ are not included.

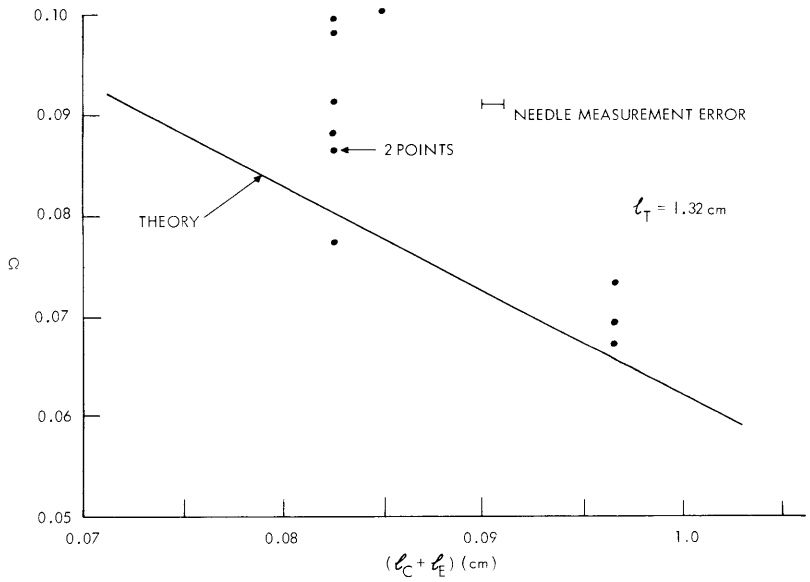

Fig. I-6. Critical velocity vs total needle length with experimental points. The fact that the points tend to lie above theory probably reflects the well-known metastability of superfluid flows.

to reduce microphonic noise. Mercury slip rings brought the signal out to the laboratory frame after being amplified by a Keithley 601 electrometer.

The procedure for each run is essentially the same: The helium is cooled to just below the lambda point where the cavity fills through superleaks. To prevent superflow induced by temperature difference, which could create vortices, the bath is slowly cooled to operating temperature and maintained there by use of a Walker regulator. At this point voltage is applied to the needle and the accelerating segment to achieve the desired levels of emission and collection current. Rotation commences after an interval to ensure that charging effects have reached steady state. The entire assembly is accelerated slowly and uniformly from rest until some arbitrary value of the angular velocity is attained, and then decelerated in the same manner. A single run takes approximately 3 hours. The emission and collection currents are monitored by strip chart recorders. An example of the decrease in collected current that we attribute to a vortex line formation between the needles is shown in Fig. I-4.

Figure I-5 is a histogram of the observed events normalized to the theoretical values of the critical angular velocities for vortex formation. The peak near 1.0 supports our predictions. Figure I-6 is a plot of the theoretical critical angular velocity as a function of total needle length with the experimental points superimposed. We note that these points fall above the theoretical values, which is to be expected because of the well-known metastability of superfluid helium flows. Additional confirmation was obtained by making runs to just below the calculated values of the critical angular velocities; in these runs no vortex formation was seen (there is one exception, see Fig. I-5). As final evidence, we note that above 1.74°K there is no appreciable trapping of electrons by vortex lines.[6,7] Absence of trapping precludes our observation of vortex formation and, as expected, we observed no vortex formations in runs with $T \geq 1.74$°K. From these data we believe that we have successfully observed vortex-line formation between the needles.

We wish to thank M. G. R. Thomson, J. G. King, F. J. O'Brien, and A. E. Berg for valuable discussions and assistance.

References

1. W. F. Vinen, Proc. Roy. Soc. (London) A260, 218 (1961).
2. G. W. Rayfield and F. Reif, Phys. Rev. Letters 11, 305 (1963).
3. R. E. Packard and T. M. Sanders, Jr., Phys. Rev. Letters 22, 823 (1969).
4. S. R. Jost, S. B. and S. M. Thesis, Department of Physics, M. I. T., May 1972.
5. S. R. Jost and J. C. Weaver, Quarterly Progress Report No. 104, Research Laboratory of Electronics, M. I. T., January 15, 1972, p. 28.
6. R. L. Douglass, Phys. Rev. Letters 13, 791 (1964).
7. R. J. Donnelly, Experimental Superfluidity (University of Chicago Press, Chicago, Ill., 1967), Chap. 6.

D. SURVIVAL OF FROG SKIN EXPOSED TO VACUUM

Joint Services Electronics Programs (Contract DAAB07-71-C-0300)
NIH (Grant 1 PO1 HL14322-01)

J. Abrams, J. A. Jarrell, J. G. King, J. C. Weaver

We have continued our preliminary experiments on frog skin,[1] exposed to vacuum through a buffering layer of Nuclepore filter material (General Electric Company, Pleasanton, California) or, more recently, directly through a single small ($\sim 10^{-2}$ cm) hole in a thin stainless-steel or plastic sheet. Our goal is to find techniques that allow frog skin and other transporting tissue to transport molecules such as H_2O, CO_2, or O_2 from a standard bathing medium (Ringer's solution) on one side of the tissue to a vacuum on the other side. The evaporating molecules can be detected individually with ionizing detectors, which operate only in vacuum. The ability to detect and count individual molecules ultimately promises high sensitivity. We can, for example, expect to detect a flux of 5×10^{10} molecules s^{-1} cm^{-2} or 10^{-1} picomoles s^{-1} cm^{-2} with intrinsic time resolution of 10^{-4} s.

The major difficulty in this new approach to transport studies lies in developing techniques for mounting and maintaining the tissue sample. The majority of our sample survival studies have been conducted with frog skin that is interfaced to the vacuum with Nuclepore filter material and which is mounted by either an "O" ring technique (Fig. I-7a) or a tissue adhesive technique (Fig. I-7b). In these studies the following procedure was used: Rana pipiens was doubly pithed. The abdominal skin was excised and rinsed well with Ringer's solution; (in this case sodium chloride 110 mM, potassium bicarbonate 2.5 mM, calcium chloride 1.0 mM, and glucose 10.0 mM, pH 8.2). When an "O" ring seal was used, the frog skin was clamped between the "O" ring and a plexiglas disk in a mounting jig. While in the mounting jig, the frog skin was bathed on its normal internal (functionally serosal) surface by Ringer's solution. The skin was then trimmed to a roughly circular shape of 0.5 in. diameter. A plexiglas screw cap maintained pressure on the "O" ring seal during potential measurements and vacuum exposure (Fig. I-7a, I-7c). In some cases, the Nuclepore stack was glued at the edge with epoxy resin (Table I-1). When we used Eastman 910 as a short-term tissue adhesive, the mounting technique was different. The skin was placed in a mounting jig that allowed us to bathe the skin on both sides with Ringer's solution. The skin was simply brought into contact with the plexiglas mounting piece: no extra pressure was applied. The skin was not trimmed to fit the plexiglas mounting piece; rather, the excess skin was blotted dry. Eastman 910 was applied to the edge of contact between the frog skin and the plexiglas mounting piece (Fig. I-7b). The only seal between the frog skin and the plexiglas mount came from the adhesive. Open-circuit potentials were measured with agar bridges constructed with 3 M KCl, calomel electrodes, and a Keithley 600B electrometer.

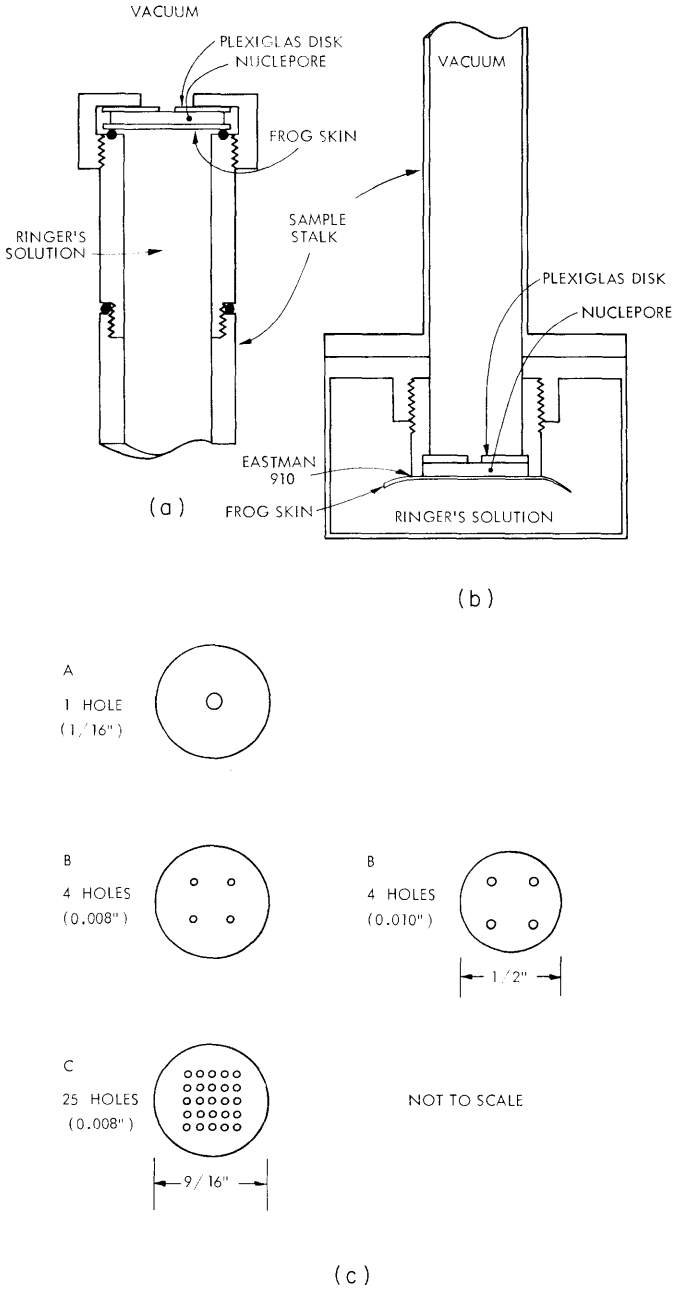

Fig. I-7. Frog skin mounting configuration.

Table I-1. Effect of vacuum on open-circuit potential developed by frog skin. Vacuum seal: "O" ring.

Trial	(See Fig. I-7) No. Layers	Pore Size (μm)	Glued	Plexiglas disk	Max. Frog Skin Potential (mV)	Frog Skin Potential Before Vacuum	Time in Vacuum (min)	Minimum Pressure (μm)	Frog Skin Potential After Vacuum (mV)	Frog Skin Potential Before ADH (mV)	Minimum Frog Skin Potential After ADH	Maximum Frog Skin Potential After ADH	Change in Frog Skin Potential (mV)	% Change	Time for Initial Response (min)
10/11/71	1	1.0	No	A	40.4	–	–	–	–	34.4	32.4	45.4	13.0	47	6.5
10/12/71	1	1.0	No	A	37.4	–	–	–	–	23.4	19.4	26.2	6.8	35	18.3
10/20/71	30	0.2	No	B	27.3	24.1	60	80	53	36	35	41	6.0	17	5.9
10/29/71	30	0.2	Yes	C	40	40	60	100	5.4	4.2	3.6	6.6	3.0	84	6-11
11/2/71	30	0.2	Yes	B	8.0	8.0	60	280	11.4	11.1	8.2	8.8	0.6	7.3	18-20
11/2/71	30	0.2	Yes	B	13.8	13.6	60	80	2.6	2.4	1.8	1.8	0	–	–
11/6/71	30	0.2	Yes	B	18.1	18.1	60	75	8.5	8.5	8.5	18.2	9.7	112	14.8
11/9/71	30	0.2	Yes	B	22.4	21.6	60	52	13.8	13.8	11.6	15.0	3.4	29	24.7
11/12/71	30	0.2	Yes	A	72	64	60	62	40	40	36	46	10	26	<6

Table I-2. Potential developed and effect of ADH on potential developed by frog skin mounted in Ussing chamber with Eastman 910 adhesive. Nuclepore not used. Solution present on both sides.

Trial	Initial Frog Skin Potential (mV)	Max. Frog Skin Potential (mV)	Final Frog Skin Potential (mV)	Frog Skin Potential Before ADH (mV)	Min. Frog Skin Potential After ADH	Max. Frog Skin Potential After ADH	Change in Frog Skin Potential (mV)	% Change	Time of Initial Response (min)
3/1/72	49	51	49	—	—	—	—	—	—
3/8/72	59	59	29	—	—	—	—	—	—
3/12/72	119	119	92	78	66	92	26	39	16.8
3/7/72	40	40	15	19	19	20	0.8	4	0.9

Table I-3. Potential developed and effect of vacuum on potential developed by frog skin mounted with Eastman 910 adhesive. The Nuclepore stack was not glued. Plexiglas disk B (Fig. I-7) was used for all trials. Vacuum seal: Eastman 910.

Trial	(See Fig. I-7) No. Layers	Pore Size (μm)	Max. Frog Skin Potential (mV)	Frog Skin Potential Before Vacuum	Time in Vacuum (min)	Minimum Pressure (μm)	Min. Frog Skin Potential After Vacuum (mV)	Max. Frog Skin Potential After Vacuum (mV)	Frog Skin Potential Before ADH (mV)	Minimum Frog Skin Potential After ADH	Maximum Frog Skin Potential After ADH	Change in Frog Skin Potential (mV)	% Change	Time for Initial Response (min)
4/26/72	30	0.2	110	110	60	200	45	85	–	–	–	–	–	–
5/2/72	30	1.0	55	48	43	200	11.8	14.0	–	–	–	–	–	–
5/4/72	20	0.2	70	52	62	25	–	51	50	50	66	16	32	8
5/5/72	30 1	0.2 1.0	79	77	94	10^{-4}	39	44	44	44	54	10	23	3
5/8/72	30 1	0.2 1.0	86	84	120	10^{-4}	–	44	44	44	44	0	–	–
5/11/72	30 1	0.2 1.0	125	128	120	10^{-4}	–	≤ 3	–	–	–	–	–	–
5/12/72	10 1	0.2 1.0	15	24	90	10^{-4}	–	8	3.4	–	–	–	–	–
5/25/72	20 1	0.2 1.0	115	80	101	10^{-4}	–	67	67	27	–	–	–	–
5/26/72	20 1	0.2 1.0	54	54	102	10^{-4}	–	60	46	46	57	11	24	10
5/30/72	20 1	0.2 1.0	95	85	123	10^{-4}	–	56	52	52	68	16	31	13
6/1/72	20 1	0.2 1.0	80	66	149	10^{-4}	–	21	26	26	35	9	–	7
6/7/72	20 1	0.2 1.0	73	50	147	10^{-4}	–	15	12.6	12.3	13.0	0.7	5.7	8.5
6/8/72	20 1	0.2 1.0	124	100	160	10^{-4}	52	69	66	–	–	–	–	–
6/12/72	50	1.0	92	73	140	10^{-4}	–	32	55	53	62	9	17	6.5

The potential developed by the frog skins was continuously recorded and the data obtained from the recordings have been tabulated in Tables I-1, I-2, and I-3. After exposure to vacuum the frog skin was removed from the apparatus. A drop of Ringer's solution was placed on the upper surface, so that the open-circuit potential could be measured. In order to make clear the effect of vacuum exposure on the potential, histograms of these

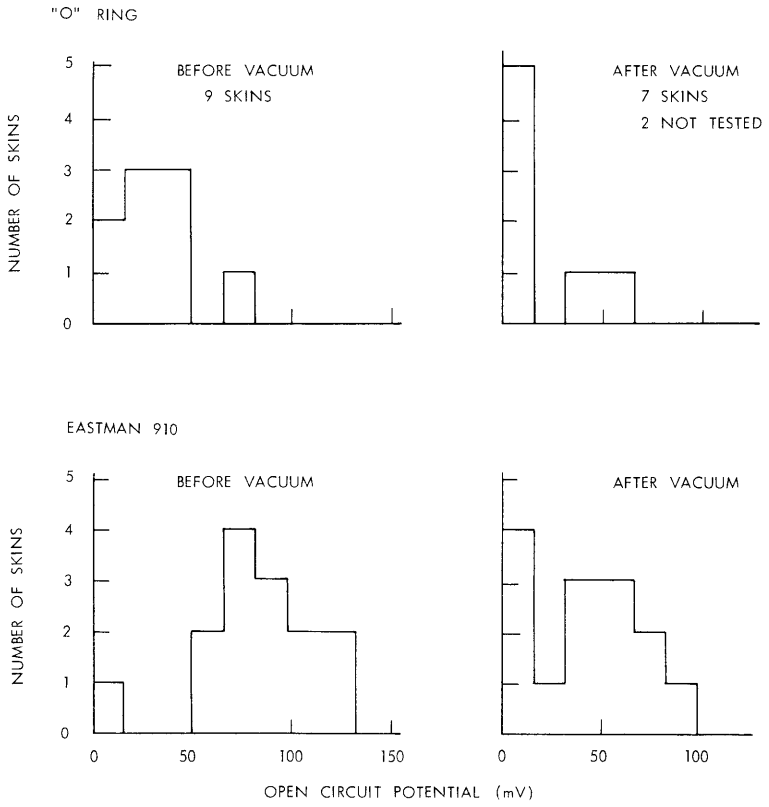

Fig. I-8. Frog skin potential.

data are shown in Fig. I-8. It is evident that in many instances the tissue survives, as indicated by the reappearance of the open-circuit potential and by its subsequent normal response to ADH (antidiuretic hormone). These results also confirm that the mounting with Eastman 910 is preferable to that with an "O" ring.[2] A more careful study is needed to establish that when we use one or more very small apertures (see Fig. I-7c), we can control the region of dehydration so that the active portion of the tissue is not affected. The recovery of the open-circuit potential and its normal response to ADH is encouraging, but we have not yet established that the active portion of the tissue below the aperture remains undamaged after exposure to vacuum. The recovered open-circuit potential may be that developed by adjacent regions, i.e., those masked from the vacuum.

Recently we have begun to use a sample preparation in which the frog skin is exposed to vacuum through a single, small ($\sim 10^{-2}$ cm^2) aperture with a single layer of Nuclepore for mechanical strength only. These tests, for the most part, are conducted in the main apparatus which is capable of H_2O flux measurement, but in this case no clear results have yet been obtained.

Throughout these experiments we have benefited from many helpful discussions with Dr. A. Essig, of Tufts Medical School and Harvard Medical School.

References

1. J. C. Weaver, J. Abrams, and J. G. King, Quarterly Progress Report No. 104, Research Laboratory of Electronics, M. I. T., January 15, 1972, p. 40.
2. S. J. Helman and D. A. Miller, Science 173, 146 (1971).

E. DESIGN OF AN ACHROMATIC COMBINED ELECTRON MIRROR AND ACCELERATING LENS

Joint Services Electronics Programs (Contract DAAB07-71-C-0300)

M. G. R. Thomson

The most serious problem encountered in image formation with low-energy electrons is the degradation of the image by chromatic aberration. If the electrons are emitted from an excited atom by the Auger process, the total energy will be of the order of 200 eV (for an element of low atomic number) and the energy spread of the order of 2 eV. This relative energy spread is 10^{-2}, and is to be compared with a figure of 10^{-5} in a high-resolution transmission electron microscope. To obtain comparable resolution, the first-order chromatic aberration of the image system must be corrected.

Achromatic lens designs have been proposed by several authors. A quadrupole and octopole design has been proposed by Rose[1] and is being carried forward by H. Koops, in Darmstadt, West Germany. A foil lens design has been described by the author[2] and by Typke.[3] The quadrupole and octopole design is extremely complicated, and involves considerable machining difficulties because of the absence of rotational symmetry. The foil design is unsuitable because the electron's energy must be at least 20 keV to pass through any feasible foil without excessive scattering. Zworykin and his co-workers used an electron mirror to correct the spherical aberration of a magnetic round lens,[4] and suggested that a mirror could also be used to correct chromatic aberration.[5]

Two approaches are possible when dealing with low-energy electrons. In the first, the electrons leave the specimen, are reflected by the electron mirror, and a greatly magnified image is formed by a lens system within which the electrons retain their 200-eV energy. The mirror design here is fairly simple, but the magnifying system, in practice,

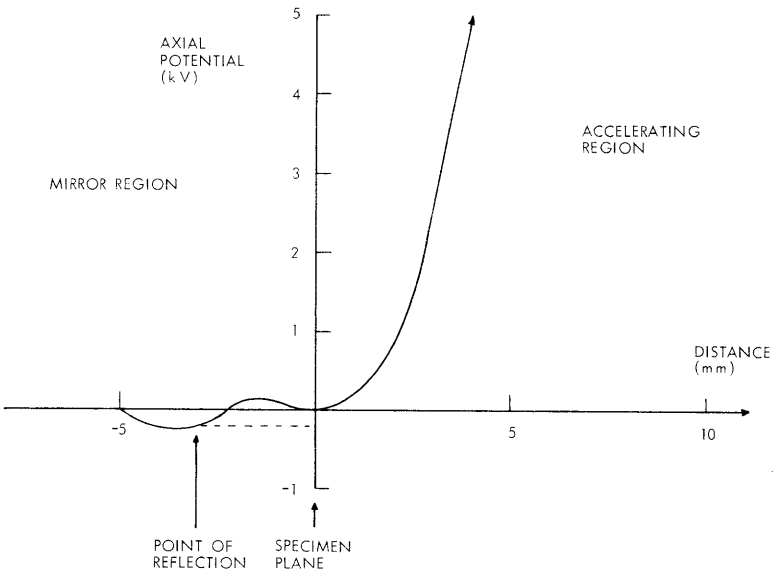

Fig. I-9. Axial potential distribution of a combined electron mirror and accelerator lens that is achromatic to first order for an electron emitted from the specimen at an energy of 200 eV. The electron is accelerated to 20 keV in the right-hand region.

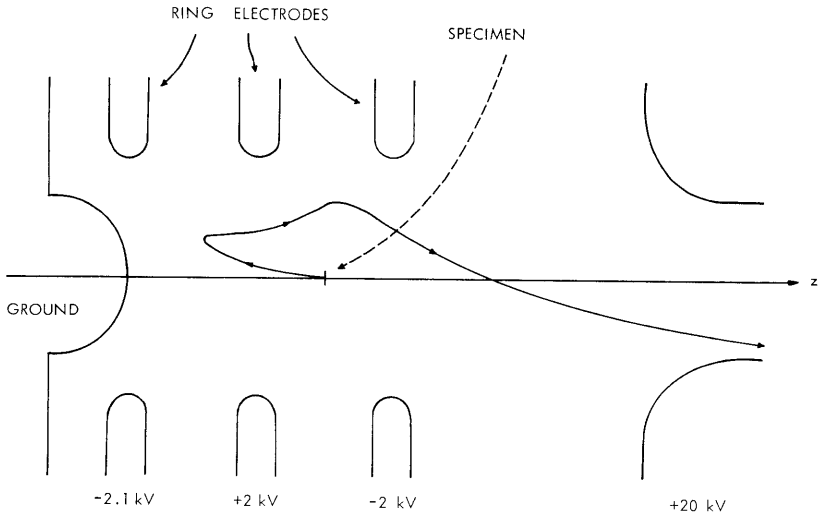

Fig. I-10. Electrode structure (with approximate potentials) for the achromatic combined electron mirror and accelerator. The specimen is at ground potential, and electrons are emitted at 200 eV. A paraxial electron trajectory is shown.

is very difficult to build (partly because of a 1% energy spread).

In the second approach the electrons, after being reflected, are accelerated to an energy of at least 20 keV. A conventional electron microscope (perhaps with a modified objective lens) can then be used to form the image. The accelerating region produces large chromatic aberration, so the electron mirror must be designed to compensate for it.

An electron mirror is a retarding electric field; the chromatic aberration is largely determined by the magnitude of the field at the point at which the electrons change direction. To make this dispersion match that of the accelerating region it has been found that the field must be made much weaker than usual. A further design constraint is imposed because the specimen has to be situated in a field-free region.

One suitable design is described in this report. The axial potential distribution is shown in Fig. I-9; the electrode design and a paraxial electron trajectory are shown in Fig. I-10. The potentials on the ring electrodes are adjusted to give zero field at the specimen and the required chromatic aberration.

A disadvantage of this system is the large spherical aberration introduced by the accelerating lens. It will probably not be possible to correct this with the mirror (under present constraints), so a foil corrector may still be necessary in the region where the electrons have higher energy. The method is also very sensitive to magnetic fields in the reflecting region where the electrons are moving at very low velocity. It will be necessary to reduce these fields to an order of a few microgauss.

The higher order chromatic and spherical aberrations are being calculated, but this requires the use of more sophisticated numerical techniques. The first experimental version will be tested on the multipurpose electron-optical bench previously described by Coleman.[6]

References

1. H. Rose, Optik 34, 285 (1971).
2. M. G. R. Thomson, Quarterly Progress Report No. 103, Research Laboratory of Electronics, M. I. T., October 15, 1971, pp. 1-5.
3. D. Typke, Optik 36, 124 (1972).
4. V. K. Zworykin, G. A. Morton, E. G. Ramberg, J. Hillier, and A. W. Vance, Electron Optics and the Electron Microscope (John Wiley and Sons, Inc., New York, 1945), p. 630.
5. Ibid, p. 643.
6. J. W. Coleman, Quarterly Progress Report No. 107, Research Laboratory of Electronics, M. I. T., October 15, 1972, pp. 1-2.